

Measurement of the Absolute Branching Fraction and Decay Asymmetry of $\Lambda \rightarrow n\gamma$

M. Ablikim,¹ M. N. Achasov,^{11,b} P. Adlarson,⁷⁰ M. Albrecht,⁴ R. Aliberti,³¹ A. Amoroso,^{69a,69c} M. R. An,³⁵ Q. An,^{66,53} X. H. Bai,⁶¹ Y. Bai,⁵² O. Bakina,³² R. Baldini Ferroli,^{26a} I. Balossino,^{27a} Y. Ban,^{42,g} V. Batozskaya,^{1,40} D. Becker,³¹ K. Begzsuren,²⁹ N. Berger,³¹ M. Bertani,^{26a} D. Bettoni,^{27a} F. Bianchi,^{69a,69c} J. Bloms,⁶³ A. Bortone,^{69a,69c} I. Boyko,³² R. A. Briere,⁵ A. Brueggemann,⁶³ H. Cai,⁷¹ X. Cai,^{1,53} A. Calcaterra,^{26a} G. F. Cao,^{1,58} N. Cao,^{1,58} S. A. Cetin,^{57a} J. F. Chang,^{1,53} W. L. Chang,^{1,58} G. Chelkov,^{32,a} C. Chen,³⁹ Chao Chen,⁵⁰ G. Chen,¹ H. S. Chen,^{1,58} M. L. Chen,^{1,53} S. J. Chen,³⁸ S. M. Chen,⁵⁶ T. Chen,¹ X. R. Chen,^{28,58} X. T. Chen,¹ Y. B. Chen,^{1,53} Z. J. Chen,^{23,h} W. S. Cheng,^{69c} S. K. Choi,⁵⁰ X. Chu,³⁹ G. Cibinetto,^{27a} F. Cossio,^{69c} J. J. Cui,⁴⁵ H. L. Dai,^{1,53} J. P. Dai,⁷³ A. Dbeyssi,¹⁷ R. E. de Boer,⁴ D. Dedovich,³² Z. Y. Deng,¹ A. Denig,³¹ I. Denysenko,³² M. Destefanis,^{69a,69c} F. De Mori,^{69a,69c} Y. Ding,³⁶ J. Dong,^{1,53} L. Y. Dong,^{1,58} M. Y. Dong,^{1,53,58} X. Dong,⁷¹ S. X. Du,⁷⁵ P. Egorov,^{32,a} Y. L. Fan,⁷¹ J. Fang,^{1,53} S. S. Fang,^{1,58} W. X. Fang,¹ Y. Fang,¹ R. Farinelli,^{27a} L. Fava,^{69b,69c} F. Feldbauer,⁴ G. Felici,^{26a} C. Q. Feng,^{66,53} J. H. Feng,⁵⁴ K. Fischer,⁶⁴ M. Fritsch,⁴ C. Fritsch,⁶³ C. D. Fu,¹ H. Gao,⁵⁸ Y. N. Gao,^{42,g} Yang Gao,^{66,53} S. Garbolino,^{69c} I. Garzia,^{27a,27b} P. T. Ge,⁷¹ Z. W. Ge,³⁸ C. Geng,⁵⁴ E. M. Gersabeck,⁶² A. Gilman,⁶⁴ K. Goetzen,¹² L. Gong,³⁶ W. X. Gong,^{1,53} W. Gradl,³¹ M. Greco,^{69a,69c} L. M. Gu,³⁸ M. H. Gu,^{1,53} Y. T. Gu,¹⁴ C. Y. Guan,^{1,58} A. Q. Guo,^{28,58} L. B. Guo,³⁷ R. P. Guo,⁴⁴ Y. P. Guo,^{10,f} A. Guskov,^{32,a} T. T. Han,⁴⁵ W. Y. Han,³⁵ X. Q. Hao,¹⁸ F. A. Harris,⁶⁰ K. K. He,⁵⁰ K. L. He,^{1,58} F. H. Heinsius,⁴ C. H. Heinz,³¹ Y. K. Heng,^{1,53,58} C. Herold,⁵⁵ M. Himmelreich,^{31,d} G. Y. Hou,^{1,58} Y. R. Hou,⁵⁸ Z. L. Hou,¹ H. M. Hu,^{1,58} J. F. Hu,^{51,i} T. Hu,^{1,53,58} Y. Hu,¹ G. S. Huang,^{66,53} K. X. Huang,⁵⁴ L. Q. Huang,⁶⁷ L. Q. Huang,^{28,58} X. T. Huang,⁴⁵ Y. P. Huang,¹ Z. Huang,^{42,g} T. Hussain,⁶⁸ N. Hüskens,^{25,31} W. Imoehl,²⁵ M. Irshad,^{66,53} J. Jackson,²⁵ S. Jaeger,⁴ S. Janchiv,²⁹ E. Jang,⁵⁰ J. H. Jeong,⁵⁰ Q. Ji,¹ Q. P. Ji,¹⁸ X. B. Ji,^{1,58} X. L. Ji,^{1,53} Y. Y. Ji,⁴⁵ Z. K. Jia,^{66,53} H. B. Jiang,⁴⁵ S. S. Jiang,³⁵ X. S. Jiang,^{1,53,58} Y. Jiang,⁵⁸ J. B. Jiao,⁴⁵ Z. Jiao,²¹ S. Jin,³⁸ Y. Jin,⁶¹ M. Q. Jing,^{1,58} T. Johansson,⁷⁰ N. Kalantar-Nayestanaki,⁵⁹ X. S. Kang,³⁶ R. Kappert,⁵⁹ M. Kavatsyuk,⁵⁹ B. C. Ke,⁷⁵ I. K. Keshk,⁴ A. Khoukaz,⁶³ P. Kiese,³¹ R. Kiuchi,¹ R. Kliemt,¹² L. Koch,³³ O. B. Kolcu,^{57a} B. Kopf,⁴ M. Kuemmel,⁴ M. Kuessner,⁴ A. Kupsc,^{40,70} W. Kühn,³³ J. J. Lane,⁶² J. S. Lange,³³ P. Larin,¹⁷ A. Lavania,²⁴ L. Lavezzi,^{69a,69c} Z. H. Lei,^{66,53} H. Leithoff,³¹ M. Lellmann,³¹ T. Lenz,³¹ C. Li,³⁹ C. Li,⁴³ C. H. Li,³⁵ Cheng Li,^{66,53} D. M. Li,⁷⁵ F. Li,^{1,53} G. Li,¹ H. Li,⁴⁷ H. Li,^{66,53} H. B. Li,^{1,58} H. J. Li,¹⁸ H. N. Li,^{51,i} J. Q. Li,⁴ J. S. Li,⁵⁴ J. W. Li,⁴⁵ Ke Li,¹ L. J. Li,¹ L. K. Li,¹ Lei Li,³ M. H. Li,³⁹ P. R. Li,^{34,j,k} S. X. Li,¹⁰ S. Y. Li,⁵⁶ T. Li,⁴⁵ W. D. Li,^{1,58} W. G. Li,¹ X. H. Li,^{66,53} X. L. Li,⁴⁵ Xiaoyu Li,^{1,58} H. Liang,^{66,53} H. Liang,³⁰ H. Liang,^{1,58} Y. F. Liang,⁴⁹ Y. T. Liang,^{28,58} G. R. Liao,¹³ L. Z. Liao,⁴⁵ J. Libby,²⁴ A. Limphirat,⁵⁵ C. X. Lin,⁵⁴ D. X. Lin,^{28,58} T. Lin,¹ B. J. Liu,¹ C. X. Liu,¹ D. Liu,^{17,66} F. H. Liu,⁴⁸ Fang Liu,¹ Feng Liu,⁶ G. M. Liu,^{51,i} H. Liu,^{34,j,k} H. B. Liu,¹⁴ H. M. Liu,^{1,58} Huanhuan Liu,¹ Huihui Liu,¹⁹ J. B. Liu,^{66,53} J. L. Liu,⁶⁷ J. Y. Liu,^{1,58} K. Liu,¹ K. Y. Liu,³⁶ Ke Liu,²⁰ L. Liu,^{66,53} Lu Liu,³⁹ M. H. Liu,^{10,f} P. L. Liu,¹ Q. Liu,⁵⁸ S. B. Liu,^{66,53} T. Liu,^{10,f} W. K. Liu,³⁹ W. M. Liu,^{66,53} X. Liu,^{34,j,k} Y. Liu,^{34,j,k} Y. B. Liu,³⁹ Z. A. Liu,^{1,53,58} Z. Q. Liu,⁴⁵ X. C. Lou,^{1,53,58} F. X. Lu,⁵⁴ H. J. Lu,²¹ J. G. Lu,^{1,53} X. L. Lu,¹ Y. Lu,⁷ Y. P. Lu,^{1,53} Z. H. Lu,¹ C. L. Luo,³⁷ M. X. Luo,⁷⁴ T. Luo,^{10,f} X. L. Luo,^{1,53} X. R. Lyu,⁵⁸ Y. F. Lyu,³⁹ F. C. Ma,³⁶ H. L. Ma,¹ L. L. Ma,⁴⁵ M. M. Ma,^{1,58} Q. M. Ma,¹ R. Q. Ma,^{1,58} R. T. Ma,⁵⁸ X. Y. Ma,^{1,53} Y. Ma,^{42,g} F. E. Maas,¹⁷ M. Maggiora,^{69a,69c} S. Maldaner,⁴ S. Malde,⁶⁴ Q. A. Malik,⁶⁸ A. Mangoni,^{26b} Y. J. Mao,^{42,g} Z. P. Mao,¹ S. Marcello,^{69a,69c} Z. X. Meng,⁶¹ J. Messchendorp,^{12,59} G. Mezzadri,^{27a} H. Miao,¹ T. J. Min,³⁸ R. E. Mitchell,²⁵ X. H. Mo,^{1,53,58} N. Yu. Muchnoi,^{11,b} Y. Nefedov,³² F. Nerling,^{17,d} I. B. Nikolaev,^{11,b} Z. Ning,^{1,53} S. Nisar,^{9,i} Y. Niu,⁴⁵ S. L. Olsen,⁵⁸ Q. Ouyang,^{1,53,58} S. Pacetti,^{26b,26c} X. Pan,^{10,f} Y. Pan,⁵² A. Pathak,³⁰ M. Pelizaeus,⁴ H. P. Peng,^{66,53} K. Peters,^{12,d} J. L. Ping,³⁷ R. G. Ping,^{1,58} S. Plura,³¹ S. Pogodin,³² V. Prasad,^{66,53} F. Z. Qi,¹ H. Qi,^{66,53} H. R. Qi,⁵⁶ M. Qi,³⁸ T. Y. Qi,^{10,f} S. Qian,^{1,53} W. B. Qian,⁵⁸ Z. Qian,⁵⁴ C. F. Qiao,⁵⁸ J. J. Qin,⁶⁷ L. Q. Qin,¹³ X. P. Qin,^{10,f} X. S. Qin,⁴⁵ Z. H. Qin,^{1,53} J. F. Qiu,¹ S. Q. Qu,⁵⁶ S. Q. Qu,³⁹ K. H. Rashid,⁶⁸ C. F. Redmer,³¹ K. J. Ren,³⁵ A. Rivetti,^{69c} V. Rodin,⁵⁹ M. Rolo,^{69c} G. Rong,^{1,58} Ch. Rosner,¹⁷ S. N. Ruan,³⁹ H. S. Sang,⁶⁶ A. Sarantsev,^{32,c} Y. Schelhaas,³¹ C. Schnier,⁴ K. Schoenning,⁷⁰ M. Scodreggio,^{27a,27b} K. Y. Shan,^{10,f} W. Shan,²² X. Y. Shan,^{66,53} J. F. Shanguan,⁵⁰ L. G. Shao,^{1,58} M. Shao,^{66,53} C. P. Shen,^{10,f} H. F. Shen,^{1,58} X. Y. Shen,^{1,58} B. A. Shi,⁵⁸ H. C. Shi,^{66,53} J. Y. Shi,¹ Q. Q. Shi,⁵⁰ R. S. Shi,^{1,58} X. Shi,^{1,53} X. D. Shi,^{66,53} J. J. Song,¹⁸ W. M. Song,^{30,1} Y. X. Song,^{42,g} S. Sosio,^{69a,69c} S. Spataro,^{69a,69c} F. Stieler,³¹ K. X. Su,⁷¹ P. P. Su,⁵⁰ Y. J. Su,⁵⁸ G. X. Sun,¹ H. Sun,⁵⁸ H. K. Sun,¹ J. F. Sun,¹⁸ L. Sun,⁷¹ S. S. Sun,^{1,58} T. Sun,^{1,58} W. Y. Sun,³⁰ X. Sun,^{23,h} Y. J. Sun,^{66,53} Y. Z. Sun,¹ Z. T. Sun,⁴⁵ Y. H. Tan,⁷¹ Y. X. Tan,^{66,53} C. J. Tang,⁴⁹ G. Y. Tang,¹ J. Tang,⁵⁴ L. Y. Tao,⁶⁷ Q. T. Tao,²³ M. Tat,⁶⁴ J. X. Teng,^{66,53} V. Thoren,⁷⁰ W. H. Tian,⁴⁷ Y. Tian,^{28,58} I. Uman,^{57b} B. Wang,¹ B. L. Wang,⁵⁸ C. W. Wang,³⁸ D. Y. Wang,^{42,g} F. Wang,⁶⁷ H. J. Wang,^{34,j,k} H. P. Wang,^{1,58} K. Wang,^{1,53} L. L. Wang,¹ M. Wang,⁴⁵ M. Z. Wang,^{42,g} Meng Wang,^{1,58} S. Wang,^{10,f} S. Wang,¹³ T. Wang,^{10,f} T. J. Wang,³⁹ W. Wang,⁵⁴ W. H. Wang,⁷¹ W. P. Wang,^{66,53} X. Wang,^{42,g} X. F. Wang,^{34,j,k} X. L. Wang,^{10,f} Y. Wang,⁵⁶ Y. D. Wang,⁴¹ Y. F. Wang,^{1,53,58} Y. H. Wang,⁴³ Y. Q. Wang,¹ Yaqian Wang,^{16,1}

Z. Wang,^{1,53} Z. Y. Wang,^{1,58} Ziyi Wang,⁵⁸ D. H. Wei,¹³ F. Weidner,⁶³ S. P. Wen,¹ D. J. White,⁶² U. Wiedner,⁴ G. Wilkinson,⁶⁴ M. Wolke,⁷⁰ L. Wollenberg,⁴ J. F. Wu,^{1,58} L. H. Wu,¹ L. J. Wu,^{1,58} X. Wu,^{10,f} X. H. Wu,³⁰ Y. Wu,⁶⁶ Y. J. Wu,²⁸ Z. Wu,^{1,53} L. Xia,^{66,53} T. Xiang,^{42,g} D. Xiao,^{34,j,k} G. Y. Xiao,³⁸ H. Xiao,^{10,f} S. Y. Xiao,¹ Y. L. Xiao,^{10,f} Z. J. Xiao,³⁷ C. Xie,³⁸ X. H. Xie,⁴² Y. Xie,⁴⁵ Y. G. Xie,^{1,53} Y. H. Xie,⁶ Z. P. Xie,^{66,53} T. Y. Xing,^{1,58} C. F. Xu,¹ C. J. Xu,⁵⁴ G. F. Xu,¹ H. Y. Xu,⁶¹ Q. J. Xu,¹⁵ X. P. Xu,⁵⁰ Y. C. Xu,⁵⁸ Z. P. Xu,³⁸ F. Yan,^{10,f} L. Yan,^{10,f} W. B. Yan,^{66,53} W. C. Yan,⁷⁵ H. J. Yang,^{46,e} H. L. Yang,³⁰ H. X. Yang,¹ L. Yang,⁴⁷ S. L. Yang,⁵⁸ Tao Yang,¹ Y. F. Yang,³⁹ Y. X. Yang,^{1,58} Yifan Yang,^{1,58} M. Ye,^{1,53} M. H. Ye,⁸ J. H. Yin,¹ Z. Y. You,⁵⁴ B. X. Yu,^{1,53,58} C. X. Yu,³⁹ G. Yu,^{1,58} T. Yu,⁶⁷ C. Z. Yuan,^{1,58} L. Yuan,² S. C. Yuan,¹ X. Q. Yuan,¹ Y. Yuan,^{1,58} Z. Y. Yuan,⁵⁴ C. X. Yue,³⁵ A. A. Zafar,⁶⁸ F. R. Zeng,⁴⁵ X. Zeng,⁶ Y. Zeng,^{23,h} Y. H. Zhan,⁵⁴ A. Q. Zhang,¹ B. L. Zhang,¹ B. X. Zhang,¹ D. H. Zhang,³⁹ G. Y. Zhang,¹⁸ H. Zhang,⁶⁶ H. H. Zhang,⁵⁴ H. H. Zhang,³⁰ H. Y. Zhang,^{1,53} J. L. Zhang,⁷² J. Q. Zhang,³⁷ J. W. Zhang,^{1,53,58} J. X. Zhang,^{34,j,k} J. Y. Zhang,¹ J. Z. Zhang,^{1,58} Jianyu Zhang,^{1,58} Jiawei Zhang,^{1,58} L. M. Zhang,⁵⁶ L. Q. Zhang,⁵⁴ Lei Zhang,³⁸ P. Zhang,¹ Q. Y. Zhang,^{35,75} Shuihan Zhang,^{1,58} Shulei Zhang,^{23,h} X. D. Zhang,⁴¹ X. M. Zhang,¹ X. Y. Zhang,⁵⁰ X. Y. Zhang,⁴⁵ Y. Zhang,⁶⁴ Y. T. Zhang,⁷⁵ Y. H. Zhang,^{1,53} Yan Zhang,^{66,53} Yao Zhang,¹ Z. H. Zhang,¹ Z. Y. Zhang,³⁹ Z. Y. Zhang,⁷¹ G. Zhao,¹ J. Zhao,³⁵ J. Y. Zhao,^{1,58} J. Z. Zhao,^{1,53} Lei Zhao,^{66,53} Ling Zhao,¹ M. G. Zhao,³⁹ Q. Zhao,¹ S. J. Zhao,⁷⁵ Y. B. Zhao,^{1,53} Y. X. Zhao,^{28,58} Z. G. Zhao,^{66,53} A. Zhemchugov,^{32,a} B. Zheng,⁶⁷ J. P. Zheng,^{1,53} Y. H. Zheng,⁵⁸ B. Zhong,³⁷ C. Zhong,⁶⁷ X. Zhong,⁵⁴ H. Zhou,⁴⁵ L. P. Zhou,^{1,58} X. Zhou,⁷¹ X. K. Zhou,⁵⁸ X. R. Zhou,^{66,53} X. Y. Zhou,³⁵ Y. Z. Zhou,^{10,f} J. Zhu,³⁹ K. Zhu,¹ K. J. Zhu,^{1,53,58} L. X. Zhu,⁵⁸ S. H. Zhu,⁶⁵ S. Q. Zhu,³⁸ T. J. Zhu,⁷² W. J. Zhu,^{10,f} Y. C. Zhu,^{66,53} Z. A. Zhu,^{1,58} B. S. Zou,¹ and J. H. Zou¹

(BESIII Collaboration)

¹*Institute of High Energy Physics, Beijing 100049, People's Republic of China*

²*Beihang University, Beijing 100191, People's Republic of China*

³*Beijing Institute of Petrochemical Technology, Beijing 102617, People's Republic of China*

⁴*Bochum Ruhr-University, D-44780 Bochum, Germany*

⁵*Carnegie Mellon University, Pittsburgh, Pennsylvania 15213, USA*

⁶*Central China Normal University, Wuhan 430079, People's Republic of China*

⁷*Central South University, Changsha 410083, People's Republic of China*

⁸*China Center of Advanced Science and Technology, Beijing 100190, People's Republic of China*

⁹*COMSATS University Islamabad, Lahore Campus, Defence Road, Off Raiwind Road, 54000 Lahore, Pakistan*

¹⁰*Fudan University, Shanghai 200433, People's Republic of China*

¹¹*G.I. Budker Institute of Nuclear Physics SB RAS (BINP), Novosibirsk 630090, Russia*

¹²*GSI Helmholtzcentre for Heavy Ion Research GmbH, D-64291 Darmstadt, Germany*

¹³*Guangxi Normal University, Guilin 541004, People's Republic of China*

¹⁴*Guangxi University, Nanning 530004, People's Republic of China*

¹⁵*Hangzhou Normal University, Hangzhou 310036, People's Republic of China*

¹⁶*Hebei University, Baoding 071002, People's Republic of China*

¹⁷*Helmholtz Institute Mainz, Staudinger Weg 18, D-55099 Mainz, Germany*

¹⁸*Henan Normal University, Xinxiang 453007, People's Republic of China*

¹⁹*Henan University of Science and Technology, Luoyang 471003, People's Republic of China*

²⁰*Henan University of Technology, Zhengzhou 450001, People's Republic of China*

²¹*Huangshan College, Huangshan 245000, People's Republic of China*

²²*Hunan Normal University, Changsha 410081, People's Republic of China*

²³*Hunan University, Changsha 410082, People's Republic of China*

²⁴*Indian Institute of Technology Madras, Chennai 600036, India*

²⁵*Indiana University, Bloomington, Indiana 47405, USA*

^{26a}*INFN Laboratori Nazionali di Frascati, INFN Laboratori Nazionali di Frascati, I-00044 Frascati, Italy*

^{26b}*INFN Sezione di Perugia, I-06100 Perugia, Italy*

^{26c}*University of Perugia, I-06100 Perugia, Italy*

^{27a}*INFN Sezione di Ferrara, INFN Sezione di Ferrara, I-44122 Ferrara, Italy*

^{27b}*University of Ferrara, I-44122 Ferrara, Italy*

²⁸*Institute of Modern Physics, Lanzhou 730000, People's Republic of China*

²⁹*Institute of Physics and Technology, Peace Avenue 54B, Ulaanbaatar 13330, Mongolia*

³⁰*Jilin University, Changchun 130012, People's Republic of China*


³¹*Johannes Gutenberg University of Mainz, Johann-Joachim-Becher-Weg 45, D-55099 Mainz, Germany*

³²*Joint Institute for Nuclear Research, 141980 Dubna, Moscow region, Russia*

³³*Justus-Liebig-Universität Giessen, II. Physikalisches Institut, Heinrich-Buff-Ring 16, D-35392 Giessen, Germany*

³⁴*Lanzhou University, Lanzhou 730000, People's Republic of China*

- ³⁵Liaoning Normal University, Dalian 116029, People's Republic of China
³⁶Liaoning University, Shenyang 110036, People's Republic of China
³⁷Nanjing Normal University, Nanjing 210023, People's Republic of China
³⁸Nanjing University, Nanjing 210093, People's Republic of China
³⁹Nankai University, Tianjin 300071, People's Republic of China
⁴⁰National Centre for Nuclear Research, Warsaw 02-093, Poland
⁴¹North China Electric Power University, Beijing 102206, People's Republic of China
⁴²Peking University, Beijing 100871, People's Republic of China
⁴³Qufu Normal University, Qufu 273165, People's Republic of China
⁴⁴Shandong Normal University, Jinan 250014, People's Republic of China
⁴⁵Shandong University, Jinan 250100, People's Republic of China
⁴⁶Shanghai Jiao Tong University, Shanghai 200240, People's Republic of China
⁴⁷Shanxi Normal University, Linfen 041004, People's Republic of China
⁴⁸Shanxi University, Taiyuan 030006, People's Republic of China
⁴⁹Sichuan University, Chengdu 610064, People's Republic of China
⁵⁰Soochow University, Suzhou 215006, People's Republic of China
⁵¹South China Normal University, Guangzhou 510006, People's Republic of China
⁵²Southeast University, Nanjing 211100, People's Republic of China
⁵³State Key Laboratory of Particle Detection and Electronics, Beijing 100049, Hefei 230026, People's Republic of China
⁵⁴Sun Yat-Sen University, Guangzhou 510275, People's Republic of China
⁵⁵Suranaree University of Technology, University Avenue 111, Nakhon Ratchasima 30000, Thailand
⁵⁶Tsinghua University, Beijing 100084, People's Republic of China
^{57a}Turkish Accelerator Center Particle Factory Group, Istinye University, 34010 Istanbul, Turkey
^{57b}Near East University, Nicosia, North Cyprus, Mersin 10, Turkey
⁵⁸University of Chinese Academy of Sciences, Beijing 100049, People's Republic of China
⁵⁹University of Groningen, NL-9747 AA Groningen, Netherlands
⁶⁰University of Hawaii, Honolulu, Hawaii 96822, USA
⁶¹University of Jinan, Jinan 250022, People's Republic of China
⁶²University of Manchester, Oxford Road, Manchester M13 9PL, United Kingdom
⁶³University of Muenster, Wilhelm-Klemm-Strasse 9, 48149 Muenster, Germany
⁶⁴University of Oxford, Keble Road, Oxford OX13RH, United Kingdom
⁶⁵University of Science and Technology Liaoning, Anshan 114051, People's Republic of China
⁶⁶University of Science and Technology of China, Hefei 230026, People's Republic of China
⁶⁷University of South China, Hengyang 421001, People's Republic of China
⁶⁸University of the Punjab, Lahore-54590, Pakistan
^{69a}University of Turin and INFN, University of Turin, I-10125 Turin, Italy
^{69b}University of Eastern Piedmont, I-15121 Alessandria, Italy
^{69c}INFN, I-10125 Turin, Italy
⁷⁰Uppsala University, Box 516, SE-75120 Uppsala, Sweden
⁷¹Wuhan University, Wuhan 430072, People's Republic of China
⁷²Xinyang Normal University, Xinyang 464000, People's Republic of China
⁷³Yunnan University, Kunming 650500, People's Republic of China
⁷⁴Zhejiang University, Hangzhou 310027, People's Republic of China
⁷⁵Zhengzhou University, Zhengzhou 450001, People's Republic of China

 (Received 23 June 2022; revised 27 September 2022; accepted 24 October 2022; published 18 November 2022)

The radiative hyperon decay $\Lambda \rightarrow n\gamma$ is studied using $(10087 \pm 44) \times 10^6 J/\psi$ events collected with the BESIII detector operating at BEPCII. The absolute branching fraction of the decay $\Lambda \rightarrow n\gamma$ is determined to be $(0.832 \pm 0.038_{\text{stat}} \pm 0.054_{\text{syst}}) \times 10^{-3}$, which is a factor of 2.1 lower and 5.6 standard deviations different than the previous measurement. By analyzing the joint angular distribution of the decay products, the first determination of the decay asymmetry α_γ is reported with a value of $-0.16 \pm 0.10_{\text{stat}} \pm 0.05_{\text{syst}}$.

DOI: [10.1103/PhysRevLett.129.212002](https://doi.org/10.1103/PhysRevLett.129.212002)

Weak radiative transitions of hadrons are governed by the interplay of the electromagnetic, weak, and strong interactions [1] and involve parity violating (p.v.) and parity conserving (p.c.) amplitudes. According to Hara's theorem [2], the p.v. amplitude of radiative hyperon decays, $B_i \rightarrow B_f \gamma$, vanishes in the limit of SU(3) flavor symmetry. Taking into account the breaking of this symmetry in the quark model, the decay asymmetry α_γ , given by the interference between p.v. and p.c. amplitudes, is expected to be positive for decays such as $\Sigma^+ \rightarrow p \gamma$, where the s quark in the initial state baryon decays to a d quark. It was, therefore, a surprise when several experiments reported a large negative value of the decay asymmetry for this process [3–7]. For other radiative hyperon decays, measurements have found nonvanishing positive decay asymmetries [8,9]. The disagreement between theoretical expectation and experimental results provoked wide interest in these processes, and various solutions to the puzzle were proposed [10–22]. It was suggested that the validity of Hara's theorem could be confirmed by determining the sign of the $\Lambda \rightarrow n \gamma$ decay asymmetry [23], a positive value indicating the theorem's violation.

In the three previous measurements of decay $\Lambda \rightarrow n \gamma$ performed by two fixed target experiments [24–26], the branching fraction (BF) was obtained from the ratio $\mathcal{B}_{\Lambda \rightarrow n \gamma} / \mathcal{B}_{\Lambda \rightarrow n \pi^0}$. Only the result from Ref. [26] is considered by the Particle Data Group (PDG) [27]. Using the electron-positron collider data, BESIII is in an excellent position to perform an absolute branching fraction measurement. Benefitting from the excellent kinematic fit technique exploiting the known energy of the initial state, the dominant background $\Lambda \rightarrow n \pi^0$ decay can be better separated than in the previous measurements. The decay asymmetry of $\Lambda \rightarrow n \gamma$, however, which is essential for the test of Hara's theorem, has not been measured so far.

At BESIII, a measurement of the $\Lambda \rightarrow n \gamma$ decay utilizing the large yield of $\Lambda \bar{\Lambda}$ pairs from $J/\psi \rightarrow \Lambda \bar{\Lambda}$ [28] is accomplished using a double-tag (DT) technique [29]. The $J/\psi \rightarrow \Lambda \bar{\Lambda}$ events are identified by reconstructing the pionic decay $\bar{\Lambda} \rightarrow \bar{p} \pi^+$ ($\Lambda \rightarrow p \pi^-$), denoted as single tag (ST). Then a DT event consisting of an ST $\bar{\Lambda}$ (Λ) candidate accompanied with a $\Lambda \rightarrow n \gamma$ ($\bar{\Lambda} \rightarrow \bar{n} \gamma$) candidate is selected. The absolute BF of the decay $\Lambda \rightarrow n \gamma$ is given by

$$\mathcal{B}_{\Lambda \rightarrow n \gamma} = \frac{N_{\text{DT}} / \varepsilon_{\text{DT}}}{N_{\text{ST}} / \varepsilon_{\text{ST}}}, \quad (1)$$

where N_{ST} (N_{DT}) and ε_{ST} (ε_{DT}) are the ST (DT) yield and the corresponding detection efficiency. Here and throughout this Letter, charge-conjugate channels are implied unless explicitly specified.

A previous BESIII study [30] showed that the Λ from $J/\psi \rightarrow \Lambda \bar{\Lambda}$ is transversely polarized with a magnitude reaching 25%. This polarization can be used to determine the decay asymmetry α_γ in the $\Lambda \rightarrow n \gamma$ decay from the

angular distribution of the daughter baryons from the $J/\psi \rightarrow \Lambda \bar{\Lambda}$ process [31]. Generally, the joint angular distribution \mathcal{W} of $J/\psi \rightarrow \bar{\Lambda} (\rightarrow \bar{p} \pi^+) \Lambda (\rightarrow n \gamma)$ can be expressed as

$$\begin{aligned} \mathcal{W}(\xi; \alpha_\psi, \Delta\Phi, \alpha_\gamma, \alpha_+) &= 1 + \alpha_\psi \cos^2 \theta_\Lambda + \alpha_\gamma \alpha_+ [\sin^2 \theta_\Lambda (n_1^x n_2^x - \alpha_\psi n_1^y n_2^y) \\ &\quad + (\cos^2 \theta_\Lambda + \alpha_\psi) n_1^z n_2^z] \\ &\quad + \alpha_\gamma \alpha_+ \sqrt{1 - \alpha_\psi^2} \cos(\Delta\Phi) \sin \theta_\Lambda \cos \theta_\Lambda (n_1^x n_2^z + n_1^z n_2^x) \\ &\quad + \sqrt{1 - \alpha_\psi^2} \sin(\Delta\Phi) \sin \theta_\Lambda \cos \theta_\Lambda (\alpha_\gamma n_1^y + \alpha_+ n_2^y), \end{aligned} \quad (2)$$

where $\hat{\mathbf{n}}_1$ ($\hat{\mathbf{n}}_2$) is the unit vector in the direction of the neutron (antiproton) in the Λ ($\bar{\Lambda}$) rest frame. The components of $\hat{\mathbf{n}}_1$ and $\hat{\mathbf{n}}_2$ are (n_1^x, n_1^y, n_1^z) and (n_2^x, n_2^y, n_2^z) , in a coordinate system where the z axis of the Λ rest frame is oriented along the momentum \mathbf{p}_Λ at an angle θ_Λ with respect to the e^- beam direction. The y axis is perpendicular to the production plane and oriented along the vector $\mathbf{p}_\Lambda \times \mathbf{k}_-$, where \mathbf{k}_- is the e^- beam momentum in the J/ψ rest frame. More details of the J/ψ rest frame can be found in Sec. I of the Supplemental Material [32]. For each event, the full set of kinematic variables $(\theta_\Lambda, \hat{\mathbf{n}}_1, \hat{\mathbf{n}}_2)$ is denoted by ξ . Furthermore, α_ψ and $\Delta\Phi$ denote the absolute ratio of the two helicity amplitudes of $J/\psi \rightarrow \Lambda \bar{\Lambda}$ and their relative phase, respectively, and α_γ (α_+) is the decay asymmetry of $\Lambda \rightarrow n \gamma$ ($\bar{\Lambda} \rightarrow \bar{p} \pi^+$). For the charge-conjugate channel, the amplitude form is identical, where the decay asymmetry of $\bar{\Lambda} \rightarrow \bar{n} \gamma$ ($\Lambda \rightarrow p \pi^-$) is denoted as $\bar{\alpha}_\gamma$ (α_-).

In this Letter, we report the absolute BF and the decay asymmetry of $\Lambda \rightarrow n \gamma$ from $(10087 \pm 44) \times 10^6$ J/ψ events [35] collected at the BESIII detector [36,37] operating at the BEPCII collider [38]. Different selection techniques are used for the charge-conjugate channels with different detection efficiencies, but leading to compatible results. Simulated data samples produced with GEANT4-based [39] Monte Carlo (MC) software, including a detailed geometric description of the BESIII detector and the detector response, are used to determine the detection efficiencies and estimate background contributions. A sample of simulated J/ψ decay events (the inclusive MC sample), corresponding to the luminosity of data, is used to study background events. Signal MC samples, including a sample of 5.6×10^7 $J/\psi \rightarrow \bar{\Lambda} (\rightarrow \bar{p} \pi^+) \Lambda (\rightarrow \text{anything})$ and a sample of 4×10^5 $J/\psi \rightarrow \bar{\Lambda} (\rightarrow \bar{p} \pi^+) \Lambda (\rightarrow n \gamma)$, are generated to estimate the ST and DT signal efficiencies, respectively. The joint angular distributions are generated according to Eq. (2), where α_γ is adopted from this analysis and $\alpha_\psi = 0.461 \pm 0.006 \pm 0.007$, $\Delta\Phi = 42.4 \pm 0.6 \pm 0.5^\circ$ and $\alpha_+ = -0.758 \pm 0.010 \pm 0.007$ from Ref. [30]. Moreover, a sample of 2×10^7 $J/\psi \rightarrow \bar{\Lambda} (\rightarrow \bar{p} \pi^+) \Lambda (\rightarrow n \pi^0)$ events is generated to study the dominant background.

The ST $\bar{\Lambda}$ candidate is reconstructed through the dominant decay mode $\bar{\Lambda} \rightarrow \bar{p}\pi^+$. Charged tracks are detected in the main drift chamber (MDC) as in Ref. [30]. The momentum ranges of pions and anti-protons from the $\bar{\Lambda}$ decays are well separated, thus the tracks with momenta less than 0.5 GeV/c are assigned to be pions, otherwise antiprotons. In addition, measurements of the specific ionization energy loss in the MDC and the flight time by the time-of-flight system are combined to perform particle identification for the (anti-)proton candidate. They are required to have the largest likelihood for the particle type selected among the pion, kaon, and proton hypotheses. Events with at least one anti-proton and one positively charged pion are selected. A vertex fit is performed to each $\bar{p}\pi^+$ pair, and the combination with the minimum χ^2_{vtx} of the vertex fit is regarded as the $\bar{\Lambda}$ candidate for further analysis. The $\bar{\Lambda}$ candidate is required to have χ^2_{vtx} less than 20, an invariant mass within 8 MeV/c² of the nominal Λ mass [27] and a decay length relative to the interaction point larger than twice its resolution.

To identify events with $J/\psi \rightarrow \Lambda\bar{\Lambda}$ and reduce the background contributions from $J/\psi \rightarrow \bar{\Lambda} + \text{anything}$ which are not due to $J/\psi \rightarrow \Lambda\bar{\Lambda}$, a recoil mass $M_{\bar{\Lambda}}^{\text{rec}} = \sqrt{(E_{\text{c.m.}} - E_{\bar{\Lambda}})^2 - P_{\bar{\Lambda}}^2}$ is defined, where $E_{\text{c.m.}}$ is the center-of-mass (c.m.) energy, $E_{\bar{\Lambda}}$ is the energy and $P_{\bar{\Lambda}}$ is the momentum of the ST $\bar{\Lambda}$ candidate. $P_{\bar{\Lambda}}$ is determined through the vertex fit of \bar{p} and π^+ . The recoil mass is required to be within $1.03 < M_{\bar{\Lambda}}^{\text{rec}} < 1.18$ GeV/c². A maximum likelihood fit of the distribution of $M_{\bar{\Lambda}}^{\text{rec}}$ is performed to determine the signal yield, which details of can be found in Sec. II of the Supplemental Material [32]. The yields of ST Λ and $\bar{\Lambda}$ candidates from the fits are summarized in Table I. The background contribution is less than 1%, which is validated by the inclusive MC sample.

On the signal side, we search for $\Lambda \rightarrow n\gamma$ decay from the residual neutral particles in the ST events. Good neutral showers in the electromagnetic calorimeter (EMC) are primarily selected as in Ref. [30]. To reject secondary showers originating from charged tracks, the shower

candidates are required to be apart from antiproton tracks with an opening angle of 20°. There are two neutral particles in the final states of the signal process. The radiative photon produces a shower in the EMC with deposited energy less than 400 MeV. With a probability of 0.65, the \bar{n} annihilates in the EMC and produces several secondary particles. The most energetic shower with an energy deposition larger than 0.4 GeV is regarded as an \bar{n} candidate. The n , meanwhile, which is difficult to identify due to its low interaction efficiency and its small energy deposition, is treated as a missing particle. Therefore, only the γ and \bar{n} are selected in this analysis. At least one shower is required as a γ candidate in an event for $\Lambda \rightarrow n\gamma$ decay, and at least two showers as γ and \bar{n} in an event for $\bar{\Lambda} \rightarrow \bar{n}\gamma$ decay. For the reconstruction of $\Lambda \rightarrow n\gamma$ decay, a one-constraint (1C) kinematic fit is applied by imposing energy-momentum conservation of the candidate particles in the hypothetical $J/\psi \rightarrow \bar{\Lambda}n\gamma$ process, where the neutron is set as a missing particle. On the other hand, for the reconstruction of $\bar{\Lambda} \rightarrow \bar{n}\gamma$ decay, the multiplicity of noise showers generated from anti-neutron is higher than that in $\Lambda \rightarrow n\gamma$ decay, a 3C kinematic fit is imposed for the $J/\psi \rightarrow \Lambda\bar{n}\gamma$ process, where the direction of the \bar{n} is measured and the energy is unmeasured. For events with multiple photon candidates, the combination giving the minimum χ^2_{1C} (χ^2_{3C}) is retained for the analysis. Furthermore, χ^2_{1C} (χ^2_{3C}) is required to be less than 10 (15).

Detailed MC studies show that the dominant background contribution comes from the $\Lambda \rightarrow n\pi^0$ decay with its large BF of 35.8% [27], while other background processes are almost negligible. The background can be classified into two categories: first, events with the detected photon from the π^0 decay, denoted as BG A, and second, events with the detected photon not from the π^0 decay, denoted as BG B. In the latter case, the photons arise from noise or a shower from secondary products of other particles. In order to suppress BG A, a 1C (3C) kinematic fit under the hypothesis $J/\psi \rightarrow \bar{\Lambda}n\gamma\gamma$ ($J/\psi \rightarrow \Lambda\bar{n}\gamma\gamma$) is performed, and events surviving the kinematic fit and with a $\gamma\gamma$ invariant mass $M_{\gamma\gamma}$ within 20 MeV/c² of the π^0 nominal mass [27] are rejected. To suppress BG B, the detected photon is required to have an energy larger than 150 MeV and an opening angle larger than 20° from the (anti-)neutron candidate. Additionally, for BG A and BG B a boosted decision tree (BDT) is applied on the detected photon to discriminate signal photons from other showers, based on the measured variables, i.e., deposited energy and its second moment, number of hits, Zernike moment (A_{42}), and deposition shape [40]. The response of the BDT output is required to be larger than 0.3, after which 86.8% (92.8%) of the BG A and 99.5% (99.7%) of the BG B events are rejected with 44.6% (48.4%) loss of the signal efficiency for the $\Lambda \rightarrow n\gamma$ ($\bar{\Lambda} \rightarrow \bar{n}\gamma$) decay.

The distribution of the photon energy in the Λ rest frame E_{γ}^{Λ} after all selection criteria is shown in Fig. 1 for the

TABLE I. The results of fits for the decays $\Lambda \rightarrow n\gamma$ and $\bar{\Lambda} \rightarrow \bar{n}\gamma$ decays. The BF and α_{γ} values are given both for individual and simultaneous fits. The first (second) uncertainties are statistical (systematic).

Decay mode	$\Lambda \rightarrow n\gamma$	$\bar{\Lambda} \rightarrow \bar{n}\gamma$
$N_{\text{ST}} (\times 10^3)$	6853.2 ± 2.6	7036.2 ± 2.7
$\epsilon_{\text{ST}} (\%)$	51.13 ± 0.01	52.53 ± 0.01
N_{DT}	723 ± 40	498 ± 41
$\epsilon_{\text{DT}} (\%)$	6.58 ± 0.04	4.32 ± 0.03
BF ($\times 10^{-3}$)	$0.820 \pm 0.045 \pm 0.066$	$0.862 \pm 0.071 \pm 0.084$
	$0.832 \pm 0.038 \pm 0.054$	
α_{γ}	$-0.13 \pm 0.13 \pm 0.03$	$0.21 \pm 0.15 \pm 0.06$
	$-0.16 \pm 0.10 \pm 0.05$	

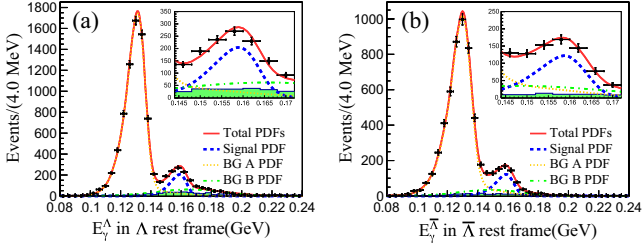


FIG. 1. Distributions of E_γ^Λ for (a) $\Lambda \rightarrow n\gamma$ and (b) $\bar{\Lambda} \rightarrow \bar{n}\gamma$ decays in the Λ and $\bar{\Lambda}$ rest frame, respectively. The black dots with error bars represent data. The red solid, blue dashed, orange dotted, and green dash-dotted lines denote the fit result, signal, BG A, and BG B contributions, respectively. The green histograms indicate the BG B from MC simulation after normalization. The insets show the details of the fit in the signal region.

decay $\Lambda \rightarrow n\gamma$ ($\bar{\Lambda} \rightarrow \bar{n}\gamma$), where the predominant peak around 0.13 GeV is from BG A, and the second peak around 0.15 GeV corresponds to the signal. To determine the DT signal yields, an unbinned extended maximum likelihood fit is performed to the E_γ^Λ distributions. The signal and BG A are modeled by the MC simulated shape convolved with a Gaussian function. Since BG B involves a fake photon and is difficult to be modeled by the MC simulation, its lineshape is obtained by a data-driven approach with a control sample of $\Lambda \rightarrow n\pi^0(\rightarrow \gamma\gamma)$ decay, and the photon candidates used in the kinematic fit are from noise photons in the EMC rather than the two signal photons from $\pi^0 \rightarrow \gamma\gamma$ decay. The DT yields obtained from fits are summarized in Table I. The BFs determined according to Eq. (1) are found to be consistent for the two charge-conjugate modes. Therefore, a simultaneous fit, assuming the same BF for the two modes, is performed, and the results are given in bold font in Table I. The total systematic uncertainty on the BF measurement is estimated to be 6.5%, including uncertainties from the photon and antineutron detection efficiency, kinematic fit, invariant $M_{\gamma\gamma}$ mass selection window, opening angle between photon and (anti-)neutron, BDT output for the photon, MC model due to the choice of α_γ , and fit procedure. It is worth noting that the dominant systematic uncertainty is from the BG B shape modeling in the fit, to be 4.8%, which is due to the limited statistics of the control sample for shape extraction. More details can be found in Sec. III of the Supplemental Material [32].

The decay asymmetry α_γ is determined using Eq. (2) with a maximum likelihood fit. A total of 1994 candidate events from charge-conjugate modes within a range of (0.145, 0.17) GeV around E_γ^Λ are used in the fit, with an estimated fraction of background events of 43.3%. In the fit of α_γ , the likelihood function of the i th event is calculated through the probability density function (PDF):

$$\mathcal{P}(\xi^i; \alpha_\psi, \Delta\Phi, \alpha_\gamma, \alpha_+) = \mathcal{C}\mathcal{W}(\xi^i; \alpha_\psi, \Delta\Phi, \alpha_\gamma, \alpha_+) \epsilon(\xi^i), \quad (3)$$

where $\mathcal{C}^{-1} = \int \mathcal{W}(\xi; \alpha_\psi, \Delta\Phi, \alpha_\gamma, \alpha_+) \epsilon(\xi) d\xi$ is the normalization factor evaluated by a phase space (PHSP) MC sample, and α_ψ , $\Delta\Phi$, α_+ are fixed to the values in Ref. [30]. The BG A and BG B contributions to the likelihood value are estimated with MC samples and subtracted in the calculation of the likelihood function. We fit the $\Lambda \rightarrow n\gamma$ and $\bar{\Lambda} \rightarrow \bar{n}\gamma$ decay modes individually, and the results agree within statistical uncertainties as summarized in Table I. A simultaneous fit, assuming the same magnitude of α_γ but with opposite signs for the charge-conjugate modes, is used to determine the decay asymmetry, yielding $\alpha_\gamma(\Lambda \rightarrow n\gamma) = -0.16 \pm 0.10$, where the uncertainty is statistical. The polarization is strongly dependent on the Λ direction $\cos\theta_\Lambda$ and indicates the amplitude of the decay asymmetry. The n_1^y (n_2^y) moment

$$\mu(\cos\theta_\Lambda) = \frac{m}{N} \sum_{i=1}^{N_k} n_{1(2)}^y, \quad (4)$$

is proportional to the product of the Λ polarization and its decay asymmetry. It is calculated for $m = 10$ bins in $\cos\theta_\Lambda$. Here, N is the total number of events in the data sample, and N_k is the number of events in the k th $\cos\theta_\Lambda$ bin. Figure 2 shows the projection of the global fit together with data and PHSP MC results. The fit result for $\bar{\Lambda} \rightarrow \bar{p}\pi^+$ decay clearly deviates from the PHSP curve, while the one for $\Lambda \rightarrow n\gamma$ decay is consistent with PHSP. The difference in magnitude of the moments for $\bar{\Lambda} \rightarrow \bar{p}\pi^+$ and $\Lambda \rightarrow n\gamma$ decays implies different values of the decay asymmetries since the polarization is the same for $\bar{\Lambda}$ and Λ . The systematic

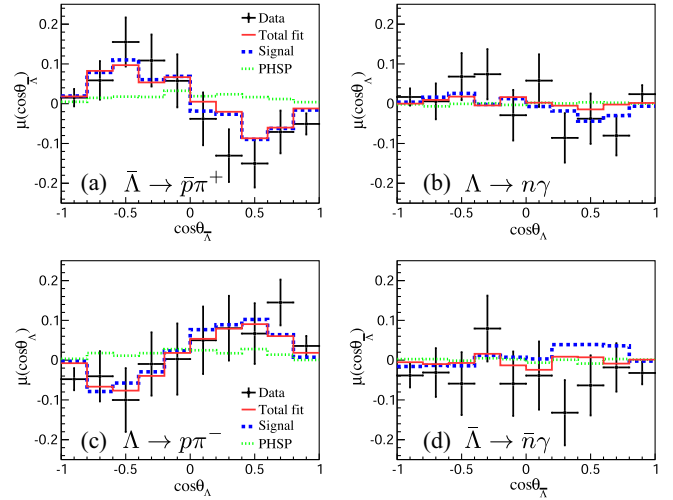


FIG. 2. Polarization moment $\mu(\cos\theta_{\Lambda(\bar{\Lambda})})$ vs $\cos\theta_{\Lambda(\bar{\Lambda})}$ for (a) $\bar{\Lambda} \rightarrow \bar{p}\pi^+$, (b) $\Lambda \rightarrow n\gamma$ decays in the process $J/\psi \rightarrow \bar{\Lambda}(\rightarrow \bar{p}\pi^+)\Lambda(\rightarrow n\gamma)$, and moment distribution $\mu(\cos\theta_{\Lambda(\bar{\Lambda})})$ vs $\cos\theta_{\Lambda(\bar{\Lambda})}$ for (c) $\Lambda \rightarrow p\pi^-$ and (d) $\bar{\Lambda} \rightarrow \bar{n}\gamma$ decays in the process $J/\psi \rightarrow \Lambda(\rightarrow p\pi^-)\bar{\Lambda}(\rightarrow \bar{n}\gamma)$. Dots with error bars indicate data and red solid lines show the fit result. The blue dashed and green dotted lines represent the moment for signal and PHSP MC, respectively.

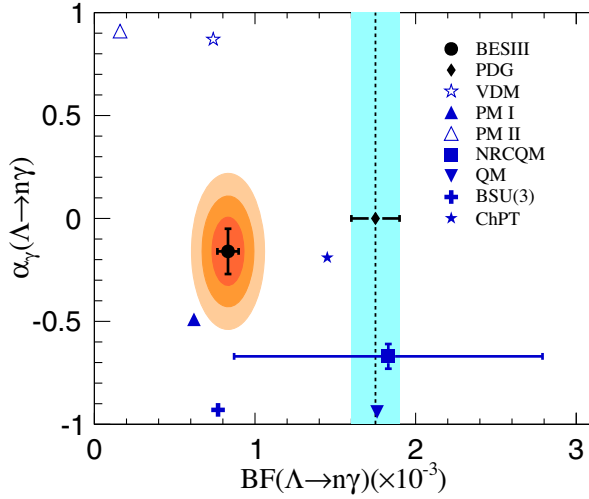


FIG. 3. Two dimensional distribution of the BF and decay asymmetry of $\Lambda \rightarrow n\gamma$ decay. The black dot and diamond with error bars denote the BESIII result and the PDG value, respectively. Other symbols in blue stand for the results predicted in the vector dominance model (VDM) [16], the pole models (PM I [17] and PM II [18]), the nonrelativistic constituent quark model (NRCQM) [19], the quark model (QM) [20], the broken SU(3) [BSU(3)] [21], and the chiral perturbation theory (ChPT) [22]. The contours in orange represent 68.2%, 95.4%, and 99.7% confidence level of the BF and α_γ .

uncertainty on α_γ is estimated to be 0.05, originating from similar sources as in the BF measurement. The main systematic uncertainty sources come from the kinematic fit, $M_{\gamma\gamma}$ mass window, opening angle between photon and (anti-)neutron, to be 0.024 or 0.022 (for 1C or 3C), 0.016, and 0.028, respectively. Detailed studies are summarized in Sec. III of the Supplemental Material [32].

In summary, we report the first absolute BF measurement result of $\Lambda \rightarrow n\gamma$ decay to be $(0.832 \pm 0.038_{\text{stat}} \pm 0.054_{\text{sys}}) \times 10^{-3}$ based on the double-tag method. As shown in Fig. 3, the measured value of the BF with improved precision, is a factor of two smaller, and 5.6 standard deviations different than the previous measurement of $(1.75 \pm 0.15) \times 10^{-3}$ [26]. By analyzing the joint angular distribution of the decay products, the decay asymmetry α_γ is determined for the first time, at a value of $-0.16 \pm 0.10_{\text{stat}} \pm 0.05_{\text{sys}}$. The BF and α_γ results of charge-conjugate modes are consistent within uncertainties, and there is no indication of any CP violation with the current dataset.

This analysis is the first measurement of radiative hyperon decays at an electron-positron collider experiment, making use of the huge number of polarized hyperons produced in J/ψ decays with clean background. The result of the decay asymmetry indicates there is no evidence that Hara's theorem does not hold for hyperon radiative decays. The decay asymmetry value does not agree well with predictions such as the Pole model [17], the broken SU(3) pole model [21] or the nonrelativistic constituent

quark model [19], which point to a large negative value. Our results are in good agreement with a recent prediction in covariant baryon ChPT [41], which can describe simultaneously the $\Xi^- \rightarrow \Sigma^- \gamma$, $\Xi^0 \rightarrow \Sigma^0 \gamma$, and $\Xi^0 \rightarrow \Lambda \gamma$ decays as well. Our BF value is consistent with the lower unitary bound obtained by considering contributions of $\Lambda \rightarrow p\pi^-$ and $\Lambda \rightarrow n\pi^0$ weak hadronic decays together with $p\pi^- \rightarrow n\gamma$ and $n\pi^0 \rightarrow n\gamma$ rescattering, respectively [42].

The BESIII Collaboration thanks the staff of BEPCII and the IHEP computing center and the supercomputing center of USTC for their strong support. The authors benefit from informative comments from Prof. Li-Sheng Geng. This work is supported in part by the National Key R&D Program of China under Contracts No. 2020YFA0406400, No. 2020YFA0406300; National Natural Science Foundation of China (NSFC) under Contracts No. 11635010, No. 11735014, No. 11835012, No. 11935015, No. 11935016, No. 11935018, No. 11961141012, No. 12022510, No. 12025502, No. 12035009, No. 12035013, No. 12192260, No. 12192261, No. 12192262, No. 12192263, No. 12192264, No. 12192265, No. 11335008, No. 11625523, No. 11705192, No. 11950410506, No. 12061131003, No. 12105276, No. 12122509; the Chinese Academy of Sciences (CAS) Large-Scale Scientific Facility Program; Joint Large-Scale Scientific Facility Funds of the NSFC and CAS under Contracts No. U1832207, No. U1732263, No. U1832103, No. U2032111; CAS Key Research Program of Frontier Sciences under Contract No. QYZDJ-SSW-SLH040; 100 Talents Program of CAS; INPAC and Shanghai Key Laboratory for Particle Physics and Cosmology; ERC under Contract No. 758462; European Union's Horizon 2020 research and innovation programme under Marie Skłodowska-Curie Grant Agreement under Contract No. 894790; German Research Foundation DFG under Contracts No. 443159800, Collaborative Research Center CRC 1044, GRK 2149; Istituto Nazionale di Fisica Nucleare, Italy; Ministry of Development of Turkey under Contract No. DPT2006K-120470; National Science and Technology fund; STFC (United Kingdom); The Royal Society, UK under Contracts No. DH140054, No. DH160214; Polish National Science Centre through the Grant No. 2019/35/O/ST2/02907; The Swedish Research Council; U.S. Department of Energy under Contract No. DE-FG02-05ER41374.

^aAlso at the Moscow Institute of Physics and Technology, Moscow 141700, Russia.

^bAlso at the Novosibirsk State University, Novosibirsk, 630090, Russia.

^cAlso at the NRC "Kurchatov Institute," PNPI, 188300, Gatchina, Russia.

^dAlso at Goethe University Frankfurt, 60323 Frankfurt am Main, Germany.

- ^cAlso at Key Laboratory for Particle Physics, Astrophysics and Cosmology, Ministry of Education; Shanghai Key Laboratory for Particle Physics and Cosmology; Institute of Nuclear and Particle Physics, Shanghai 200240, People's Republic of China.
- ^fAlso at Key Laboratory of Nuclear Physics and Ion-beam Application (MOE) and Institute of Modern Physics, Fudan University, Shanghai 200443, People's Republic of China.
- ^gAlso at State Key Laboratory of Nuclear Physics and Technology, Peking University, Beijing 100871, People's Republic of China.
- ^hAlso at School of Physics and Electronics, Hunan University, Changsha 410082, China.
- ⁱAlso at Guangdong Provincial Key Laboratory of Nuclear Science, Institute of Quantum Matter, South China Normal University, Guangzhou 510006, China.
- ^jAlso at Frontiers Science Center for Rare Isotopes, Lanzhou University, Lanzhou 730000, People's Republic of China.
- ^kAlso at Lanzhou Center for Theoretical Physics, Lanzhou University, Lanzhou 730000, People's Republic of China.
- ^lAlso at the Department of Mathematical Sciences, IBA, Karachi, Pakistan.
- [1] J. Lach and P. Zenczykowski, *Int. J. Mod. Phys. A* **10**, 3817 (1995).
- [2] Y. Hara, *Phys. Rev. Lett.* **12**, 378 (1964).
- [3] A. Manz, S. Reucroft, R. Settles, G. Wolf, J. Marraffino, C. Roos, J. Waters, and M. Webster, *Phys. Lett. B* **96B**, 217 (1980).
- [4] M. Kobayashi, J. Haba, T. Homma, H. Kawai, K. Miyake, T. S. Nakamura, N. Sasao, and Y. Sugimoto, *Phys. Rev. Lett.* **59**, 868 (1987).
- [5] L. K. Gershwin, M. Alston-Garnjost, R. O. Bangerter, A. Barbaro-Galtieri, T. S. Mast, F. T. Solmitz, and R. D. Tripp, *Phys. Rev.* **188**, 2077 (1969).
- [6] M. Foucher, I. F. Albuquerque, N. F. Bondar, R. Carrigan, D. Chen *et al.*, *Phys. Rev. Lett.* **68**, 3004 (1992).
- [7] S. Timm, I. F. Albuquerque, N. F. Bondar, R. Carrigan, D. Chen *et al.* (E761 Collaboration), *Phys. Rev. D* **51**, 4638 (1995).
- [8] C. James, K. Heller, P. Border, J. Dworkin, O. E. Overseth *et al.*, *Phys. Rev. Lett.* **64**, 843 (1990).
- [9] S. Teige *et al.*, *Phys. Rev. Lett.* **63**, 2717 (1989).
- [10] N. Vasanti, *Phys. Rev. D* **13**, 1889 (1976).
- [11] Y. I. Kogan and M. A. Shifman, *Sov. J. Nucl. Phys.* **38**, 628 (1983), <https://www-users.cse.umn.edu/~vainshte/Kogan/OnceMore/OnceMore.pdf>.
- [12] F. J. Gilman and M. B. Wise, *Phys. Rev. D* **19**, 976 (1979).
- [13] C. Goldman and C. O. Escobar, *Phys. Rev. D* **40**, 106 (1989).
- [14] M. D. Scadron and M. Visinescu, *Phys. Rev. D* **28**, 1117 (1983).
- [15] D. Palle, *Phys. Rev. D* **36**, 2863 (1987).
- [16] P. Zenczykowski, *Phys. Rev. D* **44**, 1485 (1991).
- [17] M. B. Gavela, A. Le Yaouanc, L. Oliver, O. Pene, J. C. Raynal, and T. N. Pham, *Phys. Lett.* **101B**, 417 (1981).
- [18] G. Nardulli, *Phys. Lett. B* **190**, 187 (1987).
- [19] P. Y. Niu, J. M. Richard, Q. Wang, and Q. Zhao, *Chin. Phys. C* **45**, 013101 (2021).
- [20] E. N. Dubovik, V. S. Zamiralov, S. Lepshokov, and A. E. Shkolnikov, *Phys. At. Nucl.* **71**, 136 (2008).
- [21] P. Zenczykowski, *Phys. Rev. D* **73**, 076005 (2006).
- [22] B. Borasoy and B. R. Holstein, *Phys. Rev. D* **59**, 054019 (1999).
- [23] P. Zenczykowski, *Acta Phys. Pol. B* **51**, 2111 (2020).
- [24] S. F. Biagi *et al.*, *Z. Phys. C* **30**, 201 (1986).
- [25] A. J. Noble, K. D. Larson, B. Bassalleck, W. J. Fickinger, J. R. Hall *et al.*, *Phys. Rev. Lett.* **69**, 414 (1992).
- [26] K. D. Larson, A. J. Noble, B. Bassalleck, H. Burkhardt, W. J. Fickinger *et al.*, *Phys. Rev. D* **47**, 799 (1993).
- [27] P. A. Zyla *et al.* (Particle Data Group), *Prog. Theor. Exp. Phys.* **2020**, 083C01 (2020).
- [28] H. B. Li, *Front. Phys.* **12**, 121301 (2017); **14**, 64001(E) (2019).
- [29] R. M. Baltrusaitis *et al.* (MARK-III Collaboration), *Phys. Rev. Lett.* **56**, 2140 (1986).
- [30] M. Ablikim *et al.* (BESIII Collaboration), *Nat. Phys.* **15**, 631 (2019).
- [31] G. Fäldt and A. Kupsc, *Phys. Lett. B* **772**, 16 (2017).
- [32] See Supplemental Material at <http://link.aps.org/supplemental/10.1103/PhysRevLett.129.212002> for additional details on illustration of Λ and $\bar{\Lambda}$ production in the process $e^+e^- \rightarrow J/\psi \rightarrow \Lambda\bar{\Lambda}$, fit of the distribution of the recoil mass $M_{\Lambda\bar{\Lambda}}^{\text{rec}}$, systematic uncertainties on the BF measurement and α_γ , which includes Refs. [29,33,34].
- [33] M. Ablikim *et al.* (BESIII Collaboration), *Phys. Rev. D* **83**, 112005 (2011).
- [34] L. Liu, X. Zhou, and H. Peng, *Nucl. Instrum. Methods Phys. Res., Sect. A* **1033**, 166672 (2022).
- [35] M. Ablikim *et al.* (BESIII Collaboration), *Chin. Phys. C* **46**, 074001 (2022).
- [36] M. Ablikim *et al.*, *Nucl. Instrum. Methods Phys. Res., Sect. A* **614**, 345 (2010).
- [37] M. Ablikim *et al.* (BESIII Collaboration), *Chin. Phys. C* **44**, 040001 (2020).
- [38] C. Yu *et al.*, in *7th International Particle Accelerator Conference* (JACoW, Geneva, Switzerland, 2016), p. TUYA01.
- [39] S. Agostinelli *et al.*, *Nucl. Instrum. Methods Phys. Res., Sect. A* **506**, 250 (2003).
- [40] The *deposited energy* is the total cluster energy of a shower, denoted as E_{tot} . The *hit number* is the total number of the ignited crystals of a shower. The *secondary moment* is defined as $\sum_i (E_i r_i^2 / E_{\text{tot}})$ and the *Zernike moment* (A_{42}) is defined as $|\sum_i (E_i / E_{\text{tot}}) f_{4,2}(r_i / R_0) e^{im\phi_i}|$ with the coefficient $f_{4,2} = 4x^4 - 3x^2$, where r_i and ϕ_i are the radial and angular separation of crystal i with respect to the cluster center, E_i is the i_{th} ignited crystals and R_0 is a cutoff radius of 15 cm. The deposition shape is defined as $(E_{5 \times 5} - E_{3 \times 3}) / E_{5 \times 5}$, where $E_{3 \times 3}$ and $E_{5 \times 5}$ are the deposited energies in 3×3 and 5×5 crystals around the cluster seed, respectively.
- [41] R.-X. Shi, S.-Y. Li, J.-X. Lu, and L.-S. Geng, [arXiv:2206.11773](https://arxiv.org/abs/2206.11773).
- [42] G. R. Farrar, *Phys. Rev. D* **4**, 212 (1971).